ELSEVIER

Journal of Luminescence 65 (1995) 199–209

JOURNAL OF LUMINESCENCE

Determination of oscillator strengths in $Pr^{3+}:YAlO_3$ by Raman heterodyne and hole burning spectroscopy

Tilo Blasberg, Dieter Suter*

Institute of Quantum Electronics, Swiss Federal Institute of Technology (ETH) Zürich, CH-8093 Zürich, Switzerland

Received 14 February 1995; revised 12 May 1995; accepted 12 May 1995

Abstract

The energy separation of several MHz between the nuclear spin substates of rare-earth ions in solids considerably exceeds the homogeneous width of the optical resonance lines, which is typically a few kHz. High-resolution laser experiments like coherent Raman scattering or hole burning experiments, however, can easily resolve optical transitions between individual nuclear spin states. Here, we discuss the calculation and experimental verification of the relative oscillator strengths for all possible transitions between the nuclear spin substates of the $^3H_4$ ground state and $^1D_2$ excited state of $Pr^{3+}:YAlO_3$. The oscillator strengths depend on the relative orientation of the quantization axes of the eigenstates in the ground and excited state. We determine the tensor orientation from the orientation dependence of the nuclear magnetic resonance (NMR) spectra, using Raman heterodyne detection and we use spectral hole burning to assign the orientations to the two nonequivalent lattice sites of the Pr^{3+} ions in the host lattice.

1. Introduction

Single crystals of rare earth compounds are used extensively in high-resolution coherent optical spectroscopy [1–4]. Spectral hole burning in these systems has been identified as a promising method for optical data storage [5]. The mechanism that gives rise to spectral holes is the selective depletion of nuclear spin substates of the electronic ground state of those atoms, whose resonance frequencies fall into the range selected by the laser frequency [6]. The favorable ratio between the inhomogeneous and the homogeneous line width of the optical transitions of rare-earth ions results in a high storage density.

* Corresponding author. Present address: Fachbereich Physik, Universität Dortmund, D-44221 Dortmund, Germany.

The same materials are used as laser-media [7, 8] and have been identified as attractive candidates for up-conversion-lasers [9, 10]. In all these cases, the analysis of the optical experiments relies on the correct determination of the transition matrix elements. Since the narrow homogeneous line widths of a few kHz is much smaller than the energy separation between the nuclear spin states, which is typically several MHz, a narrow bandwidth laser field interacts for each atom only with a single transition, from a specific nuclear spin state in the electronic ground state to another nuclear spin state in the electronically excited state [6, 11]. Therefore, every analysis of high-resolution laser experiments in these materials requires a detailed knowledge of the transition matrix elements for all possible transitions.

Experimental techniques for the determination of the energy-level structure include optical–radio-frequency double-resonance experiments [12–14]. These experiments can determine the energy-level structure of the rare-earth ions [6] with a frequency resolution, which is neither limited by inhomogeneous line broadening nor by laser frequency jitter and allow one to resolve individual nuclear spin substates of electronic ground or excited states. Due to the high sensitivity of these optical techniques, they represent attractive alternatives for the detection of nuclear magnetic resonance (NMR) in small or dilute samples.

This article describes the determination and verification of the relative oscillator strengths of the optical transitions between nuclear spin substates of the $^3H_4$ ground state and $^1D_2$ excited state of $Pr^{3+}:YAlO_3$ (Pr:YAP). Since the transition matrix elements are proportional to the overlap integral between the nuclear spin eigenstates [6,12], we first determined the relevant coupling constants of the nuclear spin Hamiltonian, using the radiofrequency–optical double-resonance method of Raman heterodyne detection of NMR [13]. We found that the parameter that is most important with respect to the relative oscillator strengths of Pr:YAP is the orientation of the principal axis of the effective nuclear quadrupole tensor, which determines the quantization axis of the nuclear spin Hamiltonian. We derived the orientation in both electronic states from a measurement of the dependence of the splittings between the nuclear spin substates on the orientation of an external magnetic field.

Since the Pr^{3+} ions can occupy two nonequivalent sites in the $YAlO_3$ host lattice, the analysis of the orientation-dependent NMR spectra yields two sets of nuclear spin eigenstates for the electronic ground state as well as for the electronically excited state. The eigenstates can be assigned to the two lattice sites in two different ways, which results in two different sets of optical transition matrix elements. To resolve this ambiguity, we measured the hole burning spectrum of Pr:YAP and compared it with spectra that were calculated with a simple rate-equation model. Our results clearly favor only one assignment, which has also been found previously by Mitsunaga [15].

2. Level structure and selection rules

In addition to the filled shells, the triply ionized Pr^{3+} ion has two electrons in the 4f orbitals. In the crystal field of the YAP host lattice, the remaining degeneracy of the angular momentum states is lifted completely [6]. In the following we will refer to the optical transition between the lowest crystal field states of the $^3H_4$ and $^1D_2$ multiplet as the $^3H_4 \leftrightarrow {}^1D_2$ transition. Since the interaction with the crystal field does not commute with the atomic angular momentum, the expectation value of the angular momentum operator components $\langle \Psi | J_\alpha | \Psi \rangle$ vanishes for the eigenstates Ψ of the crystal field. This effect is known as 'quenching' of the angular momentum and results in a vanishing hyperfine and electronic Zeeman interaction of the Pr^{3+} ions.

The nuclear spin of the naturally abundant isotope ^{141}Pr is $I = \frac{5}{2}$. Nuclei with spin $I > \frac{1}{2}$ have a nonspherical nuclear charge distribution, which leads to a preferential orientation of the nucleus in the inhomogeneous crystal field of the host lattice. One describes [16] this quadrupole interaction by the Hamiltonian

$$\mathcal{H}_Q = D\left[I_z^2 - \frac{I}{3}(I+1) + \frac{\eta}{3}(I_x^2 - I_y^2) \right], \qquad (1)$$

which is represented in its principal axis system. For Pr:YAP, the coupling constant D includes, in addition to the true nuclear quadrupole interaction, the so-called pseudoquadrupole interaction [17], which originates from the quenched hyperfine interaction in second order. The asymmetry parameter η describes the deviation of the quadrupole tensor from axial symmetry. In zero magnetic field, the resulting effective quadrupole interaction separates the six nuclear spin states into three groups of doubly degenerate sublevels. The sublevel splittings are of the order of 7, 14 and 21 MHz in the electronic ground state and 0.9, 1.6 and 2.5 MHz in the electronically excited state. In the axially symmetric case ($\eta = 0$), these states are simultaneously eigenstates of I_z. In the general case, however, the asymmetric part of the quadrupole interaction mixes the states within the two sets with $m_I = (\frac{5}{2}, \frac{1}{2}, -\frac{3}{2})$ and $m_I = (-\frac{5}{2}, -\frac{1}{2}, \frac{3}{2})$.

The nuclear spins interact [18] with an external magnetic field through an enhanced nuclear Zeeman interaction Hamiltonian

$$\mathcal{H}_Z = -\hbar \sum_{\alpha=x}^{z} B_\alpha \gamma_\alpha I_\alpha, \tag{2}$$

which is written in the principal axis system of the Zeeman tensor. The enhanced nuclear gyromagnetic ratios γ_α depend on the pseudoquadrupole contributions in the corresponding electronic state.

Since the interaction with the crystal field quenches the orbital angular momentum of the Pr^{3+} ion and the nuclear spin is not changed during absorption or emission of an optical photon, one can separate the electronic and nuclear spin contributions to the transition matrix elements. We write the total wave function of the ground state sublevel $|\Psi_g\rangle$ or the excited state sublevel $|\Psi_e\rangle$ as the product of an electronic part $|\phi_i\rangle$ and a nuclear spin component $|\chi_i\rangle$, where $i = (g, e)$. The transition matrix element between the two states [6, 12] becomes then

$$\langle \Psi_g | \boldsymbol{\mu} \cdot \boldsymbol{E} | \Psi_e \rangle = \langle \phi_g | \boldsymbol{\mu} \cdot \boldsymbol{E} | \phi_e \rangle \langle \chi_g | \chi_e \rangle \tag{3}$$

$$= \mu_{ge} \langle \chi_g | \chi_e \rangle . \tag{4}$$

The electronic part $\mu_{ge} = \langle \phi_g | \boldsymbol{\mu} \cdot \boldsymbol{E} | \phi_e \rangle$ of the transition matrix element is identical for all nine possible transitions of Pr:YAP. Hence the relative oscillator strengths are determined by the overlap integral $\langle \chi_g | \chi_e \rangle$ between nuclear spin eigenfunctions of different electronic configurations.

In the hypothetical case of identical quadrupole interactions in both electronic states, the nuclear spin eigenfunctions would be identical in the ground and excited state. In that case, only transitions between identical spin states would be allowed. For Pr:YAP, which has three nondegenerate nuclear spin sublevels in each electronic state, this would result in only three possible optical transitions. In reality, however, the nuclear spin eigenstates of the two electronic states differ significantly. This difference arises from two effects: As mentioned above, the asymmetric part of the nuclear quadrupole tensor, which is significantly larger in the excited state, mixes the eigenstates of I_z. In addition, the orientation of the principal axes of the quadrupole tensors is different in the two electronic states. To calculate the overlap integral (3) between nuclear spin eigenfunctions of different electronic states, one therefore has to rotate the eigenfunctions of one electronic state into the representation of the nuclear spin states of the opposite electronic state, which gives rise to an additional state mixing. As we will show in the following, this is the most important mixing effect for Pr:YAP, because the rotation angle is relatively large.

3. Quantization axes

To determine the nuclear spin eigenfunctions and their quantization axes, we used Raman heterodyne detection of NMR [13] to measure the dependence of the splittings between the nuclear spin states on the orientation of an external magnetic field. This method uses a narrow-bandwidth, resonant laser field to modify the populations of nuclear spin substates through spectral hole burning. A resonant radiofrequency (RF) field that drives a magnetic-dipole transition between two nuclear spin substates converts a laser-induced population difference between two nuclear spin states into a sublevel coherence. The same laser beam that is involved in the excitation of the sublevel coherence undergoes coherent Raman scattering [19, 20] from that coherence. The interference between the incident laser field and the coherently scattered Raman field gives rise to a heterodyne beat signal at the frequency of the RF-field that drives the sublevel transition.

The relative orientation of the quadrupole tensors in both electronic states of Pr:YAP has been determined previously by Wokaun et al. [21] and by Mitsunaga et al. [12, 15, 22]. Both experiments showed that the principal X-axis of the quadrupole tensors of both lattice sites and both electronic states coincide with the crystal c-axis. If the orientation of the quadrupole tensor of one lattice site is known, the corresponding orientation of the second lattice site can be derived from the symmetry D_{2h} of the $YAlO_3$ host lattice [23], which requires the existence of a mirror plane containing the crystal b- and c-axes. The relative orientation of the quadrupole tensors of the same lattice site but of

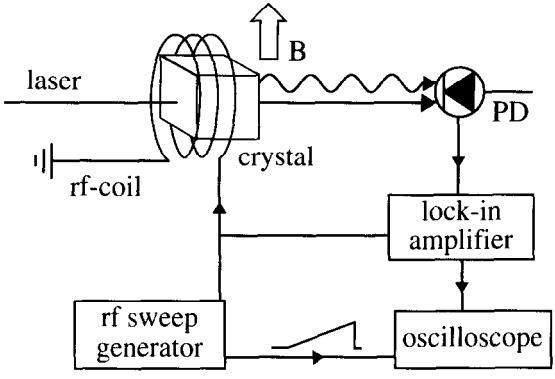

Fig. 1. Experimental setup for Raman heterodyne detection of NMR. PD: photodiode, B: external magnetic field.

different electronic states is therefore determined by a single rotation angle β between the two quantization axes in the common principal YZ plane. As explained above, the relative oscillator strengths depend on this rotation angle β.

The exact numerical value of this rotation angle has been a point of discussion. First experiments claimed that it should be only of the order of $\beta = \pm 12.8°$ [12] or $\beta = \pm 16.5°$ [21]. For such a small rotation angle, only three out of nine possible optical transitions would be of importance. However, subsequent experiments indicated that the rotation angle should be considerably larger, of the order of $\beta = 50°$ [15,24]. Since the exact numerical value of β is important for any calculation of sublevel spectra, we decided to reinvestigate the relative orientation of the quadrupole tensors. For reasons of brevity, we will discuss here only those experiments where the magnetic field was rotated in the common principal YZ plane of all quadrupole tensors.

The experiments were performed on the $^3H_4 \leftrightarrow {}^1D_2$ transition ($\lambda = 610.7$ nm) of a Pr^{3+}:YAP crystal with dimensions $5 \times 5 \times 1$ mm^3 and a Pr^{3+} concentration of 0.1 at%. Fig. 1 shows schematically the experimental setup for Raman heterodyne spectroscopy. The crystal was mounted on the cold finger of a He flow cryostat and the laser beam propagated along the crystal c-axis, parallel to the shortest crystal dimension. The RF-field ($B_{RF} \approx 1$ G, $\boldsymbol{B}_{RF} \| \boldsymbol{c}$) was created by an RF-coil in close proximity to the crystal surface. The interference between the laser field and the scattered Raman field was detected by a low-noise photodiode and a lock-in amplifier. An external magnetic field with constant field strength ($B = 40$ G) but variable orientation was produced by three orthogonal pairs of Helmholtz coils. Raman heterodyne spectra were recorded at 3 K on the electronic ground state and at 13 K on the electronically excited state.

Fig. 2 shows a typical Raman heterodyne spectrum of the $^3H_4$ $|\pm\frac{1}{2}\rangle \leftrightarrow |\pm\frac{3}{2}\rangle$ transitions of Pr:YAP. The two inserts indicate the orientation of the external magnetic and RF-field and show the relevant energy-level scheme. Since the external magnetic field is perpendicular to the principal Z-axis of lattice site 1, the nuclear spin states of site 1 are only split in second order, which results in small Zeeman splittings. The NMR transitions of this site appear close to the center of the spectrum near $\nu_{RF} = 7$ MHz. Each of the two resonance lines consists of the transitions with both $\Delta m_I = \pm 1$ and $\Delta m_I = \pm 2$, which is responsible for the larger width of these resonance lines compared to those of lattice site 2. For the second lattice site, the magnetic field is almost aligned with the principal axis of the quadrupole tensor, leading to larger Zeeman splittings. The lines near $\nu_{RF} = 7 \pm 0.4$ MHz result from transitions with $\Delta m_I = \pm 1$ and the outermost resonance lines from transitions with $\Delta m_I = \pm 2$, as indicated in the left-hand part of

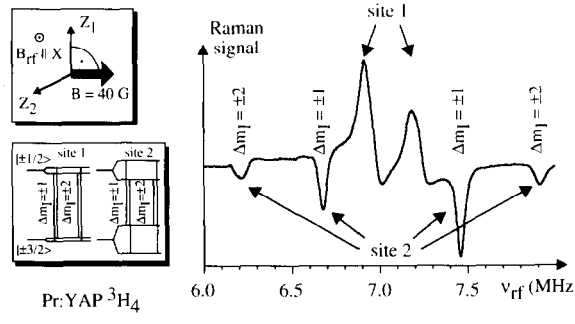

Fig. 2. Example of a Raman heterodyne spectrum of the $|\pm\frac{1}{2}\rangle \leftrightarrow |\pm\frac{3}{2}\rangle$ transitions of the electronic ground state of $Pr^{3+}:YAlO_3$. The upper insert indicates the orientation of the external magnetic field in a plane that contains the principal Y- and Z-axes of the quadrupole tensor. The lower insert explains the energy-level scheme for this orientation of the magnetic field.

Fig. 2. Although these transitions violate the selection rule $\Delta m_I = \pm 1$ of magnetic dipole transitions, they are weakly allowed, since the quadrupole interaction is slightly asymmetric, with an asymmetry parameter $\eta \approx 0.03$ in the electronic ground state.

Fig. 3 summarizes the frequencies of the $^3H_4$ $|\pm\frac{1}{2}\rangle \leftrightarrow |\pm\frac{3}{2}\rangle$ and $^1D_2$ $|\pm\frac{3}{2}\rangle \leftrightarrow |\pm\frac{5}{2}\rangle$ transitions as a function of the orientation of the external magnetic field in the principal YZ plane. Pr:YAP contains two nonequivalent lattice sites whose quadrupole tensors have different orientations. Both spectra therefore consist of two periodic data sets that are shifted by the rotation angle between the quadrupole tensors of different lattice sites.

The total spin Hamiltonian that was used for the numerical data analysis is

$$\mathcal{H} = D\left[I_z^2 - \frac{I}{3}(I+1) + \frac{\eta}{3}(I_x^2 - I_y^2)\right] - \hbar B(\gamma_x I_x \sin\Theta\cos\Phi + \gamma_y I_y \sin\Theta\sin\Phi + \gamma_z I_z \cos\Theta), \quad (5)$$

where the orientation of the external magnetic field $\boldsymbol{B}$ is given by the polar angles (Θ, ϕ). We assumed that the quantization axes of the pure nuclear quadrupole interaction and pseudoquadrupole interaction coincide. The spin Hamiltonian (5) was used to fit the quadrupole coupling constants, the enhanced gyromagnetic ratios and the relative orientation of the quadrupole tensors of the two nonequivalent lattice sites in each electronic state. The experimental data of Fig. 3 and other data, where the magnetic field was rotated in two additional planes, could be fitted with the parameters as stated in Table 1.

The transition frequencies that correspond to these fitted parameters are superimposed onto the experimental data points in Fig. 3. We note that within the experimental errors ($\pm$ 5%) the fitted gyromagnetic ratios are in good agreement with most of the published experiments on Pr:YAP [12,25].

The arrows in the two Zeeman rotation spectra of Fig. 3 indicate the orientations of the principal Z-axes of the quadrupole tensors of both lattice sites in the ground and excited state. These orientations are summarized again in the left-hand part of Fig. 4. In the electronic ground state $^3H_4$, the principal Z-axis of lattice site one (Z_1) and two (Z_2) is rotated by $\beta_0 = -56.4°$ and $\beta_0 = +56.4°$ respectively relative to the crystal b axis. In the excited state, the experiments show that the principal Z-axis of one lattice site, which we label M for the moment, is rotated by $\alpha_0 = -74.8°$ relative to the same crystal axis and the principal Z-axis (N) of the second lattice site by $\alpha_0 = +74.8°$.

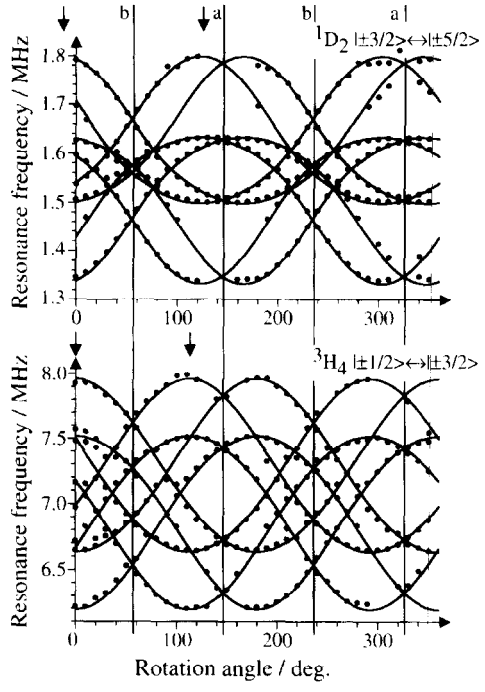

Fig. 3. Dependence of the $^1D_2$ $|\pm\frac{1}{2}\rangle \leftrightarrow |\pm\frac{3}{2}\rangle$ (top) and $^3H_4$ $|\pm\frac{1}{2}\rangle \leftrightarrow |\pm\frac{3}{2}\rangle$ (bottom) transition frequencies of Pr:YAP on the orientation of an external magnetic field in a plane that contains the principal Y- and Z-axes of all quadrupole tensors ($|\boldsymbol{B}| = 4$ mT).

Table 1

State	D (MHz)	η	$\gamma_x/2\pi$ (kHz/G)	$\gamma_y/2\pi$ (kHz/G)	$\gamma_z/2\pi$ (kHz/G)
$^3H_4$	− 3.5289	0.0100	3.5	2.43	11.05
$^1D_2$	(−) 0.4024	0.3817	1.48	1.57	1.57

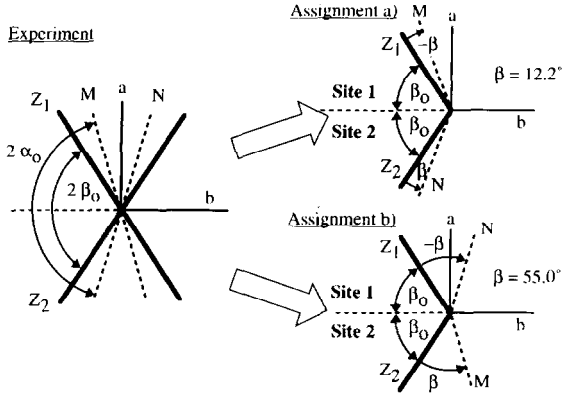

Fig. 4. Orientations of the quadrupole tensors of the two nonequivalent lattice sites of $Pr^{3+}:YAlO_3$ in the ground state (bold lines) and in the excited state (dashed lines). Two different interpretations of the Zeeman rotation spectra are possible resulting either in a small rotation angle β (assignment a), as has been assumed so far, or in a large rotation angle (assignment b).

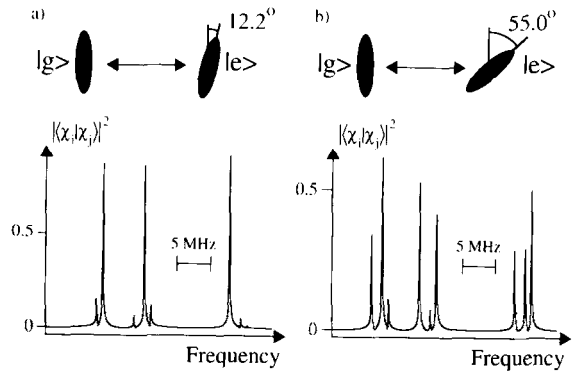

Fig. 5. Relative strengths of the optical transitions between nuclear spin substates of the ground state $^3H_4$ and excited state $^1D_2$ of $Pr^{3+}:YAlO_3$. Only three main transitions can be excited for the case of a small rotation angle β (assignment a), whereas for the larger rotation angle (assignment b) all optical transitions can be observed.

4. Assignment

From the two Zeeman rotation spectra in Fig. 3 one can derive the relative orientation of the quadrupole tensors of the two nonequivalent lattice sites either in the electronic ground state or in the excited state. However, it is not possible to derive directly from the spectra the relative orientation of the quadrupole tensors of the same lattice site but of different electronic states. This leaves us with two possible interpretations of the Zeeman rotation spectra: Either one can assume that the principal axes Z_1 and M (Z_2 and N) belong to different electronic states of lattice site 1 (2) or one can make the opposite assignment, thereby relating the principal axes Z_1 and N (Z_2 and M) to lattice site 1 (2). These two different possibilities for the assignment of the quadrupole tensors are shown on the right-hand part of Fig. 4.

For the first possible assignment, which was derived from the first experiments on Pr:YAP [12], the quadrupole tensor of the excited state is only slightly rotated with respect to the ground-state tensor (Z_i). The corresponding rotation angle of $\beta = \pm 12.2°$ that results from our experiment agrees well with published data [12]. The second possible assignment, however, corresponds to a significantly larger rotation angle of $\beta = \pm 55°$ and was favored by previous photon echo experiments [15]. Symmetry considerations do not allow us to exclude one of the two assignments, since in both cases the two lattice sites are related to each other by the same mirror plane. For both assignments, the rotation angles possess opposite values for the two lattice sites, which was a prerequisite for the analytical explanation of interference effects in Raman heterodyne detection of NMR on Pr:YAP [12].

As mentioned above, a nonvanishing rotation angle β results in a mixing of the nuclear spin eigenfunctions of the electronically excited state in the basis of the nuclear spin eigenstates of the electronic ground state. Through the overlap integral, the relative strengths of the optical transitions therefore depend critically on this rotation angle β. The theoretical spectra in the lower part of Fig. 5 summarize the relative transition strengths of Pr:YAP for the two possible rotation angles β. These spectra follow from the overlap integral (3) between nuclear spin eigenfunctions of different electronic states taking into account the quadrupole coupling constants of Eq. (5) and a rotation angle of (a) $\beta = 12.2°$ or (b) $\beta = 55.0°$. For the smaller rotation angle, only three of the nine possible transitions have significant transition strengths, since the eigenfunctions of both elec-

tronic states are almost identical. For the larger rotation angle, however, state mixing becomes significant and the spectrum changes dramatically. For the second possible assignment, $\beta = \pm 55°$, the strongest transitions are no longer those between nominally identical nuclear spin states.

Since the two optical spectra differ significantly, an additional optical experiment can help to identify the correct assignment for the relative orientation of the quadrupole tensors. Such an experimental distinction would be straightforward for a single ion, where one could compare the two calculated spectra with an experimental absorption spectrum. The large inhomogeneous line broadening in the solid, however, prevents such a direct comparison. One, therefore, has to perform an additional double-resonance experiment, which circumvents the line broadening problem. In the following section we will describe a simple rate-equation model that was used to calculate the hole burning spectrum of Pr:YAP. The comparison of calculated hole burning spectra to experimental data will then help to determine unambiguously the rotation angle β.

5. Hole burning spectrum

In hole burning spectroscopy [6,26] on rare-earth ionic solids, a narrow-bandwidth pump laser field redistributes the populations of the nuclear spin substates of the electronic ground state through optical pumping. Absorption changes due to the pump laser field are monitored by a second test laser beam whose frequency is scanned over the inhomogeneously broadened resonance line and whose intensity is sufficiently low such that it does not affect the populations. This procedure allows one to observe changes of the atomic absorption, if the frequency difference between pump and test laser beams corresponds to a sublevel splitting between two nuclear spin substates of the Pr^{3+} ion.

The energy-level structure of Pr:YAP consists of three doubly degenerate nuclear spin states in the ground and excited state, which accounts for nine possible optical transitions. Due to the large inhomogeneous line broadening, a pump laser field can simultaneously couple to all nine possible optical transitions of Pr:YAP for nine different subsets of atoms. For each of these subsets, we can describe the system with the energy-level structure indicated in Fig. 6.

Fig. 6 also explains the rate-equation model that was used for the calculation of the hole burning spectrum. A similar model has been used by Martin et al. [27] for the numerical simulation of spectral hole burning in $Ho^{3+}:LaCl_3$. For the moment, we consider spectral hole burning for only one subset of atoms where the pump laser beam couples ground-state sublevel $|2\rangle$ to the excited-state sublevel $|4\rangle$. The population changes of all four states of this model atom are given by the following set of coupled rate equations:

$$\frac{\mathrm{d}}{\mathrm{d}t}\begin{pmatrix} n_1 \\ n_2 \\ n_3 \\ n_4 \end{pmatrix} = \begin{pmatrix} -c_{12}-c_{13} & c_{12} & c_{13} & \Gamma_{41} \\ c_{12} & -c_{12}-c_{23} & c_{23} & \Gamma_{42} \\ c_{13} & c_{23} & -c_{13}-c_{23} & \Gamma_{43} \\ 0 & 0 & 0 & -\Gamma \end{pmatrix}\begin{pmatrix} n_1 \\ n_2 \\ n_3 \\ n_4 \end{pmatrix} - |\langle\chi_2|\chi_4\rangle|^2 p(n_2 - n_4)\begin{pmatrix} 0 \\ 1 \\ 0 \\ -1 \end{pmatrix}. \tag{6}$$

Here n_1, n_2, n_3 and n_4 describe the populations of the three ground-state sublevels and of the excited state respectively. The first three columns and rows of the matrix describe the spin relaxation between one nuclear spin substate of the electronic ground state and its neighboring two states. These temperature-dependent nuclear spin relaxation rates c_{ij} were measured in an independent experiment [28]. Since the sublevel splittings of Pr:YAP ($\leqslant 21$ MHz) are small as compared to typical thermal energies ($k_B T \approx 80$ GHz), the rates for upward relaxation c_{ij} and downward relaxation c_{ji} are identical.

The fourth column of the matrix describes the spontaneous decay of the excited state $|4\rangle$. As

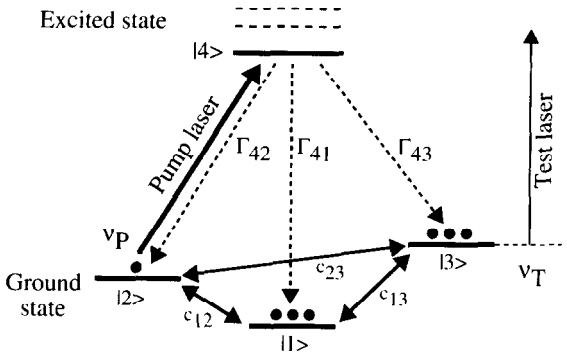

Fig. 6. Model for the calculation of hole burning spectra, including optical pumping by a pump laser beam with frequency ν_P (in this case in the transition $|2\rangle \leftrightarrow |4\rangle$), spontaneous decay of the excited state to any of the ground-state sublevels and nuclear spin relaxation in the electronic ground state. The transmission of the sample is measured by a test laser beam with variable frequency ν_T.

a first-order approximation we only took into account the spontaneous decay of the excited state to each of the three ground-state sublevels $|i\rangle$ ($i = 1, 2, 3$) with a spontaneous decay rate Γ_{4i}. These spontaneous decay rates were approximated by the overlap integral between the two nuclear spin eigenfunctions and by the excited-state lifetime T_1 ($T_1 = 180\ \mu s$ [6]):

$$\Gamma_{4i} = \frac{|\langle \chi_4 | \chi_i \rangle|^2}{T_1} \quad \text{with} \quad i \in \{1, 2, 3\}. \tag{7}$$

Since the three doubly degenerate ground-state sublevels are eigenfunctions of the quadrupole interaction and represent a complete set of basis states, the total spontaneous decay rate Γ is normalized to the inverse of T_1:

$$\Gamma = \sum_{i=1}^{3} \Gamma_{4i} = \frac{1}{T_1}. \tag{8}$$

In principle, the excited state can also decay to other crystal field states, e.g. $^3H_5$ or $^3H_6$. However, for Pr:YAP the branching ratios for the spontaneous decay to these states is still not known. As a first-order approximation we therefore neglected this additional loss mechanism for the nuclear spin memory.

The last term of Eq. (6) describes the stimulated emission and absorption of photons in the transition $|2\rangle \leftrightarrow |4\rangle$. We approximate the optical pump rate by the square of the overlap integral between two nuclear spin eigenfunctions and by a pump parameter p, which is proportional to the laser intensity and represents the only adjustable parameter in this calculation. It determines the time that is required to transfer population into the excited state. We determined the numerical value for this parameter from the transient behavior of the spectral absorption for the same pump laser intensity. For an intensity of $855\ W\,m^{-2}$ we chose a value of $p = 400\ s^{-1}$. In the numerical simulation, the main part of the population finally accumulates in the nonresonant sublevels $|1\rangle$ and $|3\rangle$ of the electronic ground state, because the excited state can decay to any of the ground-state sublevels. We obtained better results by explicitly taking into account the relaxation among the ground-state sublevels, although it is only responsible for minor contributions to the population changes.

The rate equations (6) describe the population changes only for one subset of atoms, where the pump laser field couples to the optical transition $|2\rangle \leftrightarrow |4\rangle$, as depicted in Fig. 6. Similar rate equations describe the hole burning for the remaining eight subsets of atoms. For each subset, the coupled rate equations (6) were integrated numerically, until the sublevel populations reached stationary values. For each of these nine subsets of atoms, a test laser beam with variable frequency ν_T can monitor the induced transmission changes in nine different optical transitions. Hence the total hole burning spectrum consists of 81 individual resonance lines, which coincide at various positions [29] in the spectrum. One can derive these positions from the splittings of the nuclear spin states and their energetic order. In a previous experiment [14] we could show that the quadrupole coupling constant D in the electronic ground state of Pr:YAP must be negative and found evidence for a negative sign in the excited state. We therefore assumed that the $|\pm\frac{1}{2}\rangle$ is energetically the highest sublevel of each electronic state.

If the test laser field with frequency ν_T couples to the transition $|g'\rangle \leftrightarrow |e'\rangle$ and the pump laser field with frequency ν_P to the transition $|g\rangle \leftrightarrow |e\rangle$, one can approximate the transmission change of the

sample by

$$\Delta T(\nu_T - \nu_P) = |\langle \chi_{g'} | \chi_{e'} \rangle|^2 (n_{g'}(0) - n_{g'}^{\infty}) G(\nu - \nu_0, \gamma) \tag{9}$$

with the center frequency of the resonance line

$$\nu_0 = \frac{1}{h}(E_{e'} - E_e - (E_{g'} - E_g)). \tag{10}$$

The change of the sample transmission depends on the deviation of the calculated stationary population $n_{g'}^{\infty}$ of sublevel $|g'\rangle$ from its thermal equilibrium value $n_{g'}(0) = 1/3$. In addition, the amplitude of the resonance line depends on the coupling strength of the transition $|g'\rangle \leftrightarrow |e'\rangle$. Because we are only interested in the relative signal amplitudes in the hole burning spectrum, we can replace this probability by the square of the overlap integral between the two nuclear spin eigenfunctions. In our experiments, the laser frequency jitter (≈ 0.5 MHz) was much larger than the homogeneous width of the optical transitions (≈ 5 kHz [6]). We have therefore approximated each resonance line by a Gaussian resonance line $G(\nu - \nu_0, \gamma)$ with a FWHM of $\gamma = 1$ MHz corresponding to twice the laser frequency jitter.

As the sublevel splittings in the excited state are of the same order of magnitude as the laser jitter, the hole burning spectrum of Pr:YAP consists of many resonance lines that nearly coincide at various positions. For an optimal frequency resolution in the experiments, we chose a pump and test laser intensity of 855 W m^{-2} and 20 W m^{-2} respectively and a temperature of 3 K. In the lower part of Fig. 7, the anti-holes of an experimental hole burning spectrum are compared with a calculated spectrum, assuming a rotation angle of 55°. The two insets above compare the overall shape of the experimental spectrum with two theoretical spectra, calculated for identical parameters ($T = 3$ K, $p = 400$ s^{-1}) assuming the set of relative transition strengths that results either (a) from the first assignment $\beta = \pm 55°$ or (b) from the second assignment $\beta = \pm 12.2°$.

The spectrum (b) consists of only three major anti-holes on each side of the central spectral hole, which occur at those positions, where the laser frequency difference corresponds to one of the

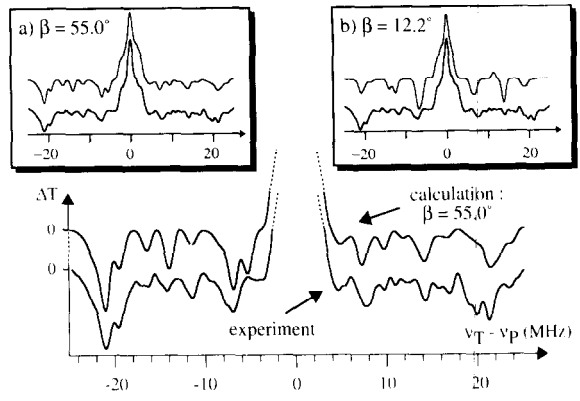

Fig. 7. Experimental and calculated hole burning spectra as a function of the frequency difference $\nu_T - \nu_P$ between the test (T) and pump (P) laser beam. The experimental spectrum is compared with two spectra, calculated (a) for the larger rotation angle β and (b) for the smaller rotation angle. The experimental spectrum clearly favors the larger rotation angle.

ground-state sublevel splittings. Between these anti-holes the transmission of the sample remains unchanged, since only the main transitions between similar nuclear spin substates are allowed for this small rotation angle. Obviously, this is not the case in the experimental spectrum. For the larger rotation angle, however, the calculated transmission change is in good agreement with the experimental spectrum at most of the spectral positions. This comparison indicates that the relative orientation of the quadrupole tensors must be $\beta = \pm 55°$, corresponding to the first assignment for the rotation angle β.

There might be several reasons for the remaining deviations of the calculated spectrum. First, we did not take into account the spontaneous decay of the excited state to other crystal field states, which can result in an additional spin flipping. Second, the proposed model for spectral hole burning does not include relaxation among the excited-state sublevels. And finally the calculation of the hole burning spectrum was not performed in the full eigenbasis of the nuclear quadrupole Hamiltonian, which consists of the $|-\frac{5}{2}\rangle, \ldots, |+\frac{5}{2}\rangle$ nuclear spin states. Instead we treated two doubly degenerate sublevels, e.g. $|-\frac{5}{2}\rangle$ and $|+\frac{5}{2}\rangle$, as a single level $|\pm\frac{5}{2}\rangle$, since the nuclear spin relaxation rates are only known in the absence of an external magnetic field [28].

6. Conclusion

The fact that the hole burning spectrum of Pr:YAP consists of many anti-holes, which overlap at various positions, is a clear proof that for this crystal most of the optical transitions are allowed, which is only possible for a large rotation angle β. The relative transition strengths are determined by the overlap integral of the nuclear spin eigenstates. Two effects contribute to significantly nonzero values: In the excited state, the quadrupole tensor deviates significantly from axial symmetry. The eigenstates of the quadrupole Hamiltonian are therefore not eigenstates of the spin operator I_z. However, as the spectrum in Fig. 6 for a small rotation angle β shows, this effect is only of minor importance. In Pr:YAP, the dominant effect, which gives rise to a strong state mixing, is the different orientation of the quadrupole tensors in the two electronic states. Our experiments clearly showed that the quadrupole tensor in the electronically excited state $^1D_2$ is rotated by $\beta = \pm 55°$ relative to the ground-state ($^3H_4$) tensor around the common X-axis. Thus our experiments clearly favor the second possible interpretation of the Zeeman rotation spectra, which has also been suggested previously by Mitsunaga and co workers [15,24].

To the best of our knowledge, this is the first calculation of a hole burning spectrum of a rare-earth ionic solid with the relative strengths of the optical transitions derived directly from the nuclear spin eigenfunctions and without the need of additional adjustable parameters. A similar calculation of hole burning spectra was also reported for the solid $Ho^{3+}:LaCl_3$ [27,30]. However, in their calculation, the authors had to fit the relative transition strengths and the spin relaxation rates from transient hole burning spectra. For a comparable numerical simulation on the related solid $Pr^{3+}:Y_2SiO_5$ [31], the authors had to assume that hole burning is equivalent for each of the nine optical transitions and applied ad hoc selection rules for the detection of the spectrum, since the relative orientation of the quadrupole tensors and hence the relative transition strengths are still unknown for this crystal.

The method of coherent Raman scattering [20] can only be applied in high-resolution laser spectroscopy if two optical transitions of an atomic Λ- or V-type three-level configuration are allowed. Pr:YAP represents an ideal model system for this method, since most of its optical transitions possess comparable oscillator strength (compare with Fig. 5). In coherent Raman scattering experiments that use a test laser beam with variable frequency, we could show that coherent Raman scattering yields comparable signal amplitudes in most of the nine different transitions of Pr:YAP (cf. Ref. [11, Fig. 8]). This is an additional evidence that the second assignment for the rotation angle β must be the correct interpretation of the Zeeman rotation spectra of Fig. 3.

The signal amplitude in Raman heterodyne detection of NMR depends on the sublevel coherence that is excited by the resonant RF-field. As in conventional NMR experiments, this sublevel coherence depends on the population difference between two nuclear spin states [13]. In RF–optical double-resonance experiments, the thermal population differences are greatly enhanced through spectral hole burning of a resonant laser field. With the proposed rate-equation model, one can calculate the populations of the individual nuclear spin substates during spectral hole burning. Thus a detailed analysis of Raman heterodyne spectra becomes possible [32,33]. Our experiments and calculations also have consequences for optical data storage by spectral hole burning in Pr:YAP. As Fig. 7 shows, the anti-holes can obtain significant amplitudes. Since these anti-holes can coincide with spectral holes of ions absorbing at a different optical frequency, this can substantially lower the depth of spectral holes and lead to interference between data stored at frequencies that differ by a nuclear sublevel splitting.

Acknowledgements

The authors gratefully acknowledge the financial support by the Schweizerischer Nationalfonds.

References

[1] R.M. MacFarlane, R.M. Shelby and R.L. Shoemaker, Phys. Rev. Lett. 43 (1979) 1726.

[2] R.G. DeVoe and R.G. Brewer, Phys. Rev. Lett. 50 (1983) 1269.
[3] A. Schenzle, R.G. DeVoe and R.G. Brewer, Phys. Rev. A 30 (1984) 1866.
[4] S. Glaser, G. Wäckerle and K. Dinse, Chem. Phys. Lett. 121 (1985) 267.
[5] M. Mitsunaga, R. Yano and N. Uesugi, Opt. Lett. 16 (1991) 1890.
[6] R.M. MacFarlane and R.M. Shelby, in: Spectroscopy of Solids Containing Rare Earth Ions, eds. A. Kaplyanskii and R.M. MacFarlane (North-Holland, Amsterdam, 1987).
[7] T. Danger, A. Bleckmann and G. Huber, Appl. Phys. B 58 (1994) 413.
[8] W. Koechner, Solid-State Laser Engineering (Springer-Verlag, Berlin, 1992).
[9] R. Brede, T. Danger, E. Heumann, G. Huber and B. Chai, Appl. Phys. Lett. 63 (1993) 729.
[10] R.R. Stephens and R.A. McFarlane, Opt. Lett. 18 (1993) 34.
[11] T. Blasberg and D. Suter, Phys. Rev. B 51 (1995) 6309.
[12] M. Mitsunaga, E.S. Kintzer and R.G. Brewer, Phys. Rev. B 31 (1985) 6947.
[13] N.C. Wong, E.S. Kintzer, J. Mlynek, R.G. DeVoe and R.G. Brewer, Phys. Rev. B 28 (1983) 4993.
[14] T. Blasberg and D. Suter, Phys. Rev. B 48 (1993) 9524.
[15] M. Mitsunaga, Phys. Rev. A 42 (1990) 1617.
[16] M.H. Cohen and F. Reif, Solid State Phys. 5 (1957) 321.
[17] M.A. Teplov, Sov. Phys. JETP 26 (1968) 872.
[18] B. Bleaney, Physica 69 (1973) 317.
[19] J.A. Giordmaine and W. Kaiser, Phys. Rev. 144 (1966) 676.
[20] R.G. Brewer and E.L. Hahn, Phys. Rev. A 8 (1973) 464.
[21] A. Wokaun, S. Rand, R.G. DeVoe and R.G. Brewer, Phys. Rev. B 23 (1981) 5733.
[22] M. Mitsunaga, E.S. Kintzer and R.G. Brewer, Phys. Rev. Lett. 52 (1984) 1484.
[23] R. Diehl and G. Brandt, Mater. Res. Bull. 10 (1975) 85.
[24] M. Mitsunaga, R. Yano and N. Uesugi, Phys. Rev. B 45 (1992) 12760.
[25] L.E. Erickson, Phys. Rev. B 24 (1981) 5388.
[26] S. Völker, Ann. Rev. Phys. Chem. 40 (1989) 499.
[27] J.P.D. Martin, N.E. Rigby and N.B. Manson, J. Lumin. 55 (1993) 31.
[28] T. Blasberg and D. Suter, Chem. Phys. Lett. 215 (1993) 668.
[29] L.E. Erickson, Phys. Rev. B 16 (1977) 4731.
[30] N.B. Manson, N. Rigby, B. Lou and J.P.D. Martin, J. Lumin. 53 (1992) 251.
[31] K. Holliday, M. Croci, E. Vauthey and U. Wild Phys. Rev. B 47 (1993) 14741.
[32] T. Blasberg and D. Suter, Phys. Rev. B 51 (1995) 12439.
[33] L.E. Erickson, Phys. Rev. B 42 (1990) 3789.